Anal. Chem. **2007,** *79,* 4215−4221

Determination of Size and Concentration of Gold Nanoparticles from UV−Vis Spectra

Wolfgang Haiss,*,†,‡ Nguyen T. K. Thanh,†,‡ Jenny Aveyard,† and David G. Fernig‡

Centre for Nanoscale Science, Department of Chemistry, University of Liverpool, Crown Street L69 7ZD, U.K., and School of Biological Sciences, University of Liverpool, Crown Street L69 7ZB, U.K.

The dependence of the optical properties of spherical gold nanoparticles on particle size and wavelength were analyzed theoretically using multipole scattering theory, where the complex refractive index of gold was corrected for the effect of a reduced mean free path of the conduction electrons in small particles. To compare these theoretical results to experimental data, gold nanoparticles in the size range of 5 to 100 nm were synthesized and characterized with TEM and UV−vis. Excellent agreement was found between theory and experiment. It is shown that the data produced here can be used to determine both size and concentration of gold nanoparticles directly from UV−vis spectra. Equations for this purpose are derived, and the precision of various methods is discussed. The major aim of this work is to provide a simple and fast method to determine size and concentration of nanoparticles.

Colloidal gold, initially produced by mechanical means, has been used for more than a thousand years for medical purposes and since a few hundred years to produce colored glasses. In 1857 Faraday reported the formation of deep red solutions upon reduction of chloroaurate ($AuCl_4^-$) with white phosphorus in a two-phase CS_2−water mixture. During the last few decades numerous procedures for the synthesis[1−4] and detection[5,6] of colloidal gold have been reported, and as recently reviewed,[7] gold nanoparticles (GNPs) nowadays have many applications in diagnostics, therapeutics, catalysis, optical sensing, and as biomarkers and building blocks in nanotechnology.

In many of these applications the optical properties of the GNPs are of primary importance. In 1908 Mie[8] presented a solution to the Maxwell equations, which facilitated the calculation of the extinction and scattering efficiencies of small metal particles. Later, Stratton[9] introduced a more formal approach, which is commonly used today.[10,11] In addition to the theoretical work, a sizable amount of experimental data have been collected, and the influence of particle size, shape, dielectric environment, and surface coatings on the extinction and scattering cross sections of small metal particles have been discussed.[11−15]

In this paper the optical properties of spherical GNPs in aqueous solutions are analyzed, both theoretically and experimentally, for diameters from 3 to 120 nm. Methods to calculate the particle diameter (d) from UV−vis spectra are derived, and analytical relations between the extinction efficiency (Q_{ext}) and d are established, which allow the determination of the particle concentration (c). The major aim is to provide researchers preparing gold hydrosols or using them with a simple and fast method to determine size and concentration. An extension of the calculations described here for alternative materials and other dielectric environments is possible, and the reader is encouraged to develop his own calibration curves using our FORTRAN 77 program, which can be found in the Supporting Information together with several tables which allow the reader to determine the size and the concentration of GNPs in aqueous solutions from UV−vis spectra without performing calculations.

METHODS

Preparation and Characterization of the Gold Hydrosols. Small GNPs with a diameter of ∼5.0 nm were prepared by the following procedure: To 90 mL of deionized water ("Millipore"), 1 mL of 1 wt % $HAuCl_4 \cdot 3H_2O$ was added, and the mixture was stirred for 1 min; then, 2 mL of 38.8 mM sodium citrate was added, and the reaction mixture was stirred for another minute. A volume of 1 mL of fresh 0.075 wt % $NaBH_4$ in 38.8 mM sodium citrate was added, and the reaction mixture was stirred for 5 min.

* To whom correspondence should be addressed. E-mail: w.h.haiss@liv.ac.uk.

† Department of Chemistry.

‡ School of Biological Sciences.

(1) Grabar, K. C.; Freeman, R. G.; Hommer, M. B.; Natan, M. J. *Anal. Chem.* **1995**, *67*, 735−743.
(2) Brown, K. R.; Walter, D. G.; Natan, M. J. *Chem. Mater.* **2000**, *12*, 306−313.
(3) Henglein, A.; Meisel, D. *Langmuir* **1998**, *14*, 7392−7396.
(4) Brust, M.; Fink, J.; Bethell, D.; Schiffrin, D. J.; Kiely, C. *J. Chem. Soc., Chem. Commun.* **1995**, 1655−1656.
(5) Berciaud, S.; Lasne, D.; Blab, G. A.; Cognet, L.; Lounis, B. *Phys. Rev. B* **2006**, *73*, 045424.
(6) Boyer, D.; Tamarat, P.; Maali, A.; Lounis, B.; Orrit, M. *Science* **2002**, *297*, 1160−1163.
(7) Daniel, M. C.; Astruc, D. *Chem. Rev.* **2004**, *104*, 293−346.
(8) Mie, G. *Ann. Phys.* **1908**, *25*, 377−445.
(9) Stratton, J. A. *Electromagnetic Theory*; McGraw-Hill: New York, 1941.
(10) Bohren, C. F.; Huffman, D. R. *Absorption and Scattering of Light by Small Particles*; Wiley-Interscience: New York, 1983.
(11) Kreibig, U.; Vollmer, M. *Optical Properties of Metal Clusters*; Springer: Berlin, 1995.
(12) Jensen, T.; Kelly, L.; Lazarides, A.; Schatz, G. C. *J. Cluster Sci.* **1999**, *10*, 295.
(13) Berciaud, S.; Cognet, L.; Tamarat, P.; Lounis, B. *Nano Lett.* **2005**, *5*, 515−518.
(14) Kelly, K. L.; Coronado, E.; Zhao, L. L.; Schatz, G. C. *J. Phys. Chem. B* **2003**, *107*, 668−677.
(15) Mulvaney, P. *Langmuir* **1996**, *12*, 788−800.

10.1021/ac0702084 CCC: $37.00
Published on Web 04/26/2007

Seed GNPs of ~17−20 nm diameter were synthesized using citrate to reduce Au^{3+} following the procedure of Grabar et al.[1] Stock solutions of 25.4 mM $HAuCl_4 \cdot 3H_2O$, 38.8 mM sodium citrate, and 0.2 M hydroxylamine−hydrochloride ($NH_2OH \cdot HCl$) were prepared in Millipore water. Since $HAuCl_4$ is corrosive, a glass spatula was used to avoid its contact with metal. We found that it was crucial that all glassware and magnetic stir bars used in these syntheses were thoroughly cleaned in aqua regia (HCl/HNO_3 3:1, v/v), rinsed in distilled water, and then oven-dried prior to use, to avoid unwanted nucleation during the synthesis, as well as aggregation of gold colloid solutions. The synthesis was performed in a 250 mL round-bottom flask equipped with a condenser to maintain a constant volume of the reaction mixture. The vigorously stirred solution (125 mL, 254 μM $HAuCl_4 \cdot 3H_2O$) was brought to boiling in a paraffin bath (at 125−150 °C). Rapid addition of 12.5 mL of 40 mM sodium citrate to the vortexed $HAuCl_4$ solution resulted in a color change from pale yellow to dark red. The color change occurred over several minutes. The solution was maintained for 10 min at boiling temperature and then removed from the heating mantle. Stirring was continued for another 15 min.

These particles were then used as seed particles for the synthesis of gold particles larger than 20 nm following a procedure developed by Brown et al.[2] In this method Au^{3+} is reduced on the surface of preformed colloidal gold at room temperature using hydroxylamine−hydrochloride ($NH_2OH \cdot HCl$) as a reducing agent:

$$HAuCl_4 + NH_2OH \cdot HCl \rightarrow Au + 5HCl + NO \qquad (1)$$

The reduction of Au^{3+} on the surface of the GNPs increases their diameter to a final value that is determined by the diameter of the seed particles and the amount of reduced Au^{3+}. A typical reaction for 35−40 nm GNPs was carried out as follows. To 270 mL of water, 30 mL of preformed seed gold particles was added, followed by the addition of 3 mL of 0.2 M $NH_2OH \cdot HCl$. The mixture was stirred vigorously at room temperature, and 2.5 mL of 25.4 mM $HAuCl_4 \cdot 3H_2O$ was added dropwise to the mixture. The color of the suspension changed to darker red concurrent with the addition of the gold salt. The reaction was completed within a minute. The resulting gold colloids were stored at 4 °C in the dark to minimize photoinduced oxidation.

All gold hydrosols were characterized using a Perkin-Elmer 25 UV−vis spectrometer in the wavelength range from 350 to 800 nm, with a resolution of 1 nm. A "FEI 120 KV Tecnai G2 Sprint BioTwin" transmission electron microscope (TEM) was used to take several pictures of each batch of particles. The diameter of at least 100 particles of each batch was determined from these TEM images to characterize the size distribution of the particles. Figure 1 shows the size distribution of GNPs having an average size of 60 ± 9 nm together with a typical TEM image as an inset. The Feret diameter of the particles, i.e., the diameter of a sphere having the equivalent surface area, was determined automatically using "Immage Tool" software. The elongation of the particles, i.e., the ratio of the long to the short axes, was typically between 1.05 and 1.25. The particles can therefore be described as spherical in good approximation.

The standard deviation of all nanoparticle sizes in a size distribution is the error in d, which is stated in the text and the figures of this paper. The number density of the particles was calculated from the total amount of gold used for the synthesis, the measured particle diameter, and the volume of the solution in which they were synthesized. Thus, the synthesis reactions were assumed to be complete, since excess amounts of reducing agent were used. This assertion was consistent with UV−vis spectroscopy in the wavelength range of 200−300 nm where no residues of H_4AuCl_4 could be detected.

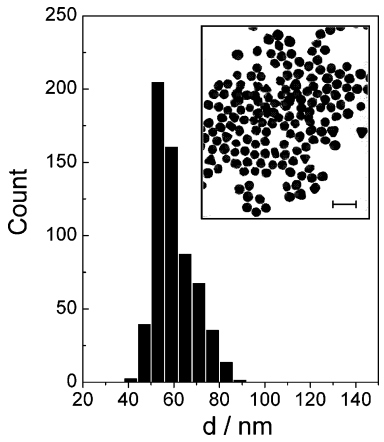

Figure 1. Size distribution of 617 GNPs with average diameter of 60 ± 9 nm. The inset shows a typical TEM image. The particles in the image have an average elongation factor of 1.12 and hence can be described as spherical in good approximation. The scale bar in the inset corresponds to 200 nm.

In addition to the nanoparticles synthesized and characterized by the procedures described above, commercial GNPs (BBInternational) were also analyzed for comparison. Size and number density of these nanoparticles were obtained from the manufacturer's datasheet. To facilitate a distinction between the two types of particles, results obtained from the commercial nanoparticles are symbolized with down triangles, whereas the results obtained from in-house synthesized nanoparticles are symbolized with up triangles in all figures.

Theoretical Calculations. The extinction cross section σ_{ext} of a spherical particle with radius R embedded in a medium with dielectric function ϵ_m at a wavelength λ can be represented by[10,11]

$$\sigma_{ext} = \frac{2\pi}{|k|^2} \sum (2L + 1) \mathrm{Re}(a_L + b_L) \qquad (2)$$

Here, $k = 2\pi\sqrt{\epsilon_m}/\lambda$ is the wave vector, $a_L(R, \lambda)$ and $b_L(R, \lambda)$ are the scattering coefficients in terms of Ricatti−Bessel functions ($\eta_L(x)$ and $\psi_L(x)$), which are defined by eqs 3a and 3b.

$$a_L = \frac{m\psi_L(mx)\psi_L'(x) - \psi_L'(mx)\psi_L(x)}{m\psi_L(mx)\eta_L'(x) - \psi_L'(mx)\eta_L(x)} \qquad (3a)$$

$$b_L = \frac{\psi_L(mx)\psi_L'(x) - m\psi_L'(mx)\psi_L(x)}{\psi_L(mx)\eta_L'(x) - m\psi_L'(mx)\eta_L(x)} \qquad (3b)$$

$x = kR$ is the size parameter and $m = n/n_m$, where n is the complex refractive index of the particle and n_m is the real refractive index of the surrounding medium. For very small particles, i.e., for $x \ll 1$, the electric field is approximately homogeneous within areas of the particle dimension, and it is sufficient to take into

account only the first electric dipole term (i.e., $L = 1$ in eq 3). Since a large range of particle sizes were analyzed, multipole terms have also been taken into account throughout.

For the numerical calculation of the extinction efficiency Q_{ext} ($Q_{ext} = \sigma_{ext}/\pi R^2$) the original FORTRAN code of Bohren and Huffman was used, which can be found in the appendix of ref 10, together with computational details. The complex refractive index $n(\lambda)$ for bulk gold was taken from the experimental work of Johnson and Christy,[16] where the original data were fitted with a spline-fit to enable the calculation of Q_{ext} over a continuous range of λ. All calculations were performed with water at 20 °C as the surrounding medium where a wavelength-independent refractive index was assumed ($n_{med} = 1.333$). The calculated value for the extinction efficiency can be related to the experimentally observed absorption (A) by eq 4 via the number density of particles per unit volume N and the path length of the spectrometer (d_0), which is usually 1 cm.

$$A = \frac{\pi R^2 Q_{ext} d_0 N}{2.303} \tag{4}$$

Since the optical functions of gold are dependent on the particle size for particle sizes smaller than the mean free path in bulk gold, we have corrected n for the influence of a reduced mean free path of the conduction electrons. This was done in the framework of the extended Drude model following the arguments brought forward in ref 17. In brief, the complex dielectric constant ϵ ($\epsilon = n^2$) is split into contributions from the bound electrons (B_1 and B_2) and contributions from the free electrons ($A_1(R)$ and $A_2(R)$) according to eq 5. These contributions are shown in Figure 2.

$$\epsilon(R) = \epsilon_1(R) + i\epsilon_2(R) = (A_1(R) + B_1) + i(A_2(R) + B_2) \tag{5}$$

with

$$A_1 = 1 - \frac{{\omega_P}^2}{\omega^2 + {\omega_0}^2} \tag{5a}$$

and

$$A_2 = \frac{{\omega_P}^2 \omega_0}{\omega(\omega^2 + {\omega_0}^2)} \tag{5b}$$

The plasma frequency ω_P and the collision frequency ω_0 are defined as

$$\omega_0 = 1/\tau_s \tag{6}$$

and

$$\omega_P = (4\pi N_e e^2/m^*) \tag{7}$$

Here, τ_s is the static collision time ($\tau_s = 3 \times 10^{-14}$ s for bulk gold[18]), N_e is the density of conduction electrons, e is the electron charge, and m^* is the effective mass of the conduction electron. The mean free path of the conduction electrons in the bulk ($l_\infty \sim 42$ nm for gold) is simply the product of τ_s and the Fermi velocity (v_F). In small particles the mean free path is reduced due to collisions of electrons with the particle surface, which is represented by an additional contribution τ_c to the collision time, where $\tau_c = R/v_F$,[19] and hence the dependence of the mean free path on R for a small spherical particle is given by

$$l(R)^{-1} = l_\infty^{-1} + R^{-1} \tag{8}$$

To take this effect into account, $\omega_0(R)$ ($\omega_0(R) = \omega_0 + v_F/R$) is calculated and the contributions of the free electrons to the dielectric constants are recalculated according to eqs 5a and 5b using $\omega_0(R)$ instead of ω_0. If not stated otherwise, all results for $Q_{ext}(R, \lambda)$ shown in this paper were calculated using optical functions corrected for the mean free path effect by this procedure, and typical results for $\epsilon_1(R)$ and $\epsilon_2(R)$ are shown in Figure 3.

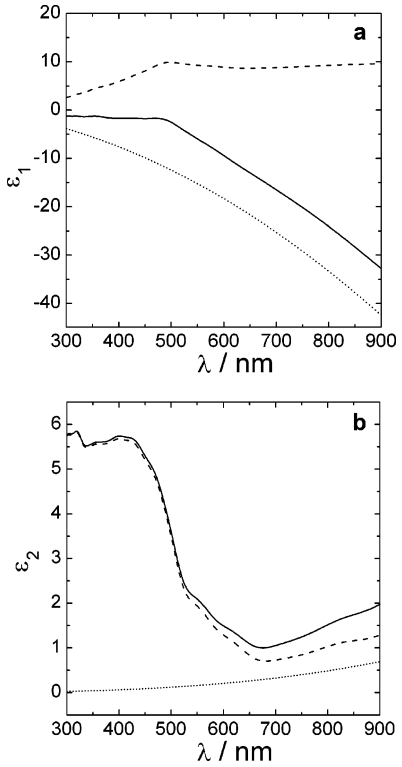

Figure 2. Contributions of the bound electrons (dashed lines) and the free electrons (dotted lines) to the dielectric functions (solid lines) ϵ_1 (a) and ϵ_2 (b) of bulk gold.

RESULTS AND DISCUSSION

In Figure 4a, the extinction efficiency (Q_{ext}) in dependence on λ for particle diameters between 2.5 and 100 nm is shown. The surface plasmon resonance (spr) is clearly visible as a peak in the range between 520 and 580 nm. For small particles this peak is damped due to the reduced mean free path of the electrons. This gets clearer in Figure 4b, where the mean free path corrected results for a particle diameter of 20.4 nm (dotted line) are compared to calculations where no correction was applied (dashed line).

(16) Johnson, P. B.; Christy, R. W. *Phys. Rev. B* **1972**, *6*, 4370−4379.
(17) Kreibig, U.; Vonfrags. C *Z. Phys.* **1969**, *224*, 307.
(18) Ashcroft, N. W.; Mermin, N. D. *Solid State Physics*; Hartcourt Brace Collage Publishers: New York, 1976.
(19) Euler, J. *Z. Phys.* **1954**, *137*, 318.

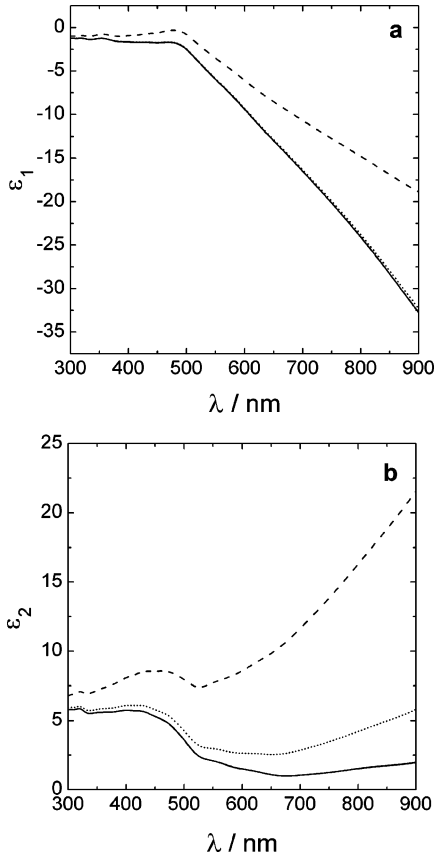

Figure 3. Dielectric function ϵ_1 (a) and ϵ_2 (b) for spherical gold particles in dependence of the particle size ($R = 1$ nm, dashed line; $R = 7.5$ nm, dotted line; bulk gold, solid line).

The agreement between experimental data (solid line in Figure 4b) and mean free path corrected theory is excellent, especially as the absorption was calculated quantitatively from size and concentration of the particles without any adjustable parameter.

The calculated position of the surface plasmon peak as displayed in Figure 5 (circles) is in perfect agreement with the experimental data (triangles in Figure 5) for particle sizes from 25 to 120 nm. For sizes smaller than 25 nm the experimentally observed peak position is somewhat lower than predicted by theory. This may be attributed to the pronounced increase of the ratio of surface atoms to bulk atoms for particle diameters smaller than 20 nm. However, for sizes larger than 25 nm both the theoretical and the experimental peak positions (λ_{spr}) are both fitted precisely by a simple exponential function ($R^2 = 0.99$, see the dotted and the dashed lines in Figure 5):

$$\lambda_{spr} = \lambda_0 + L_1 \exp(L_2 d) \tag{9}$$

Particle diameters (d) ranging from 35 to 100 nm can thus be calculated from the peak position according to eq 10:

$$d = \frac{\ln\left(\frac{\lambda_{spr} - \lambda_0}{L_1}\right)}{L_2} \tag{10}$$

With the use of the fit parameters determined from the theoretical values for $d > 25$ nm ($\lambda_0 = 512$; $L_1 = 6.53$; $L_2 = 0.0216$) the average

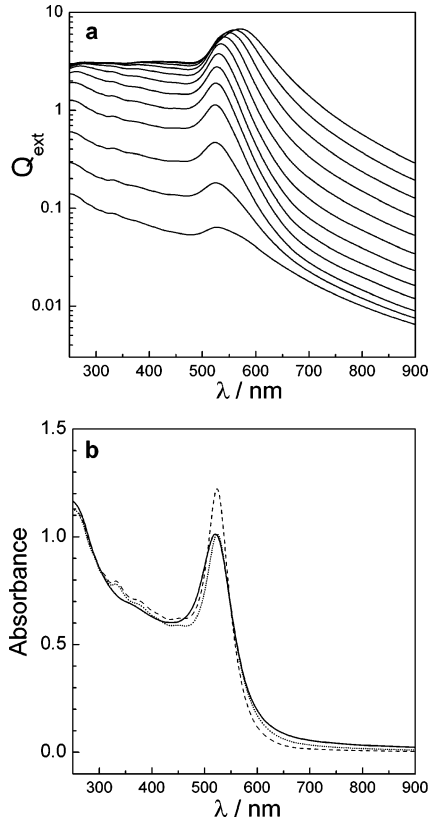

Figure 4. (a) Calculated extinction efficiency (Q_{ext}) in dependence of λ for particle diameters of 2.5, 5, 10, 20, 30, 40, 50, 60, 70, 80, 90, 100 nm (from bottom to top). (b) Comparison of the calculated absorbance (dotted line) with the experimentally measured absorbance (solid line) for a particle diameter of 20.4 nm and a particle concentration of 10^{-9} M. The results of a calculation using the optical functions of bulk gold are shown for comparison (dashed line).

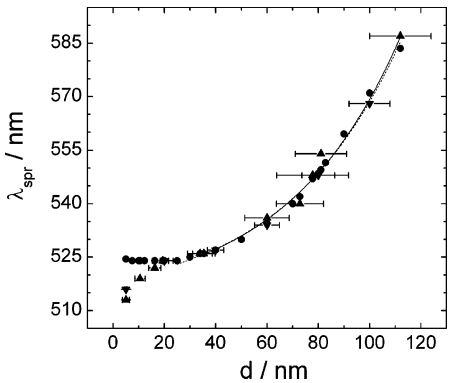

Figure 5. Position of the surface plasmon resonance peak (λ_{spr}) as a function of the particle diameter for GNPs in water: calculated (circles); experimentally measured (downward-pointing triangles, commercial GNPs; upward-pointing triangles, in-house synthesized GNPs). An exponential fit to the theoretical (experimental) data for $d > 25$ nm is shown as a dotted (dashed) line.

of the absolute error in calculating the experimentally observed particle diameters is only 3%, and hence eq 10 allows a precise determination of d in the range of 35−110 nm. Numerical data of $d(\lambda_{spr})$ which allow the reader to determine the size of GNPs without the need to perform calculations are presented in the Supporting Information.

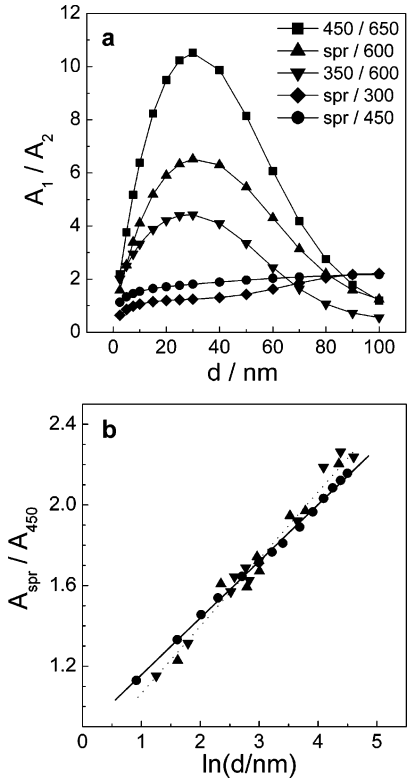

Figure 6. (a) Calculated ratios of absorbance values of gold spheres in dependence of their diameter. (b) Ratio of the absorbance of GNPs at the surface plasma resonance peak (A_{spr}) to the absorbance at 450 nm (A_{450}) in dependence of the logarithm of the particle diameter: theory (spheres); experiment (triangles). A linear fit of the theoretical (experimental) data is shown as dotted (solid) line.

The size of GNPs with diameters smaller than 35 nm cannot be determined using eq 10, and hence another method has to be employed in this size range. Since, for decreasing particle size, A_{spr} is increasingly damped relative to the absorbance at other wavelengths, the *ratio* of the absorbance at different wavelengths may be used to determine the particle size without knowledge of the concentration. Figure 6a shows theoretical results for the ratio of absorbance (A_1/A_2) of GNPs in dependence of the particle diameter, where the wavelengths are stated in the figure; for example, 450/600 refers to A_1 at $\lambda = 450$ nm divided by A_2 at $\lambda = 650$ nm.

The most pronounced dependence of A_1/A_2 on d is found if A_2 is taken in the long-wavelength range. This is of course due to the pronounced influence of the mean free path on the long-wavelength region of the optical functions (compare Figure 3). It was found that in the long-wavelength range for some hydrosols the calculated absorbance was not in good agreement with the measured absorbance. This is probably due to the presence of small amounts of oblate particles or particle aggregates in some of the sols, which typically show strong absorbance at longer wavelengths.[14,20−22] From this viewpoint the ratios from Figure 6a, which have long-wavelength values in the denominator, can be used to ascertain the quality of the gold hydrosol or monitor aggregation of particles but are not suitable for the determination of particle sizes.

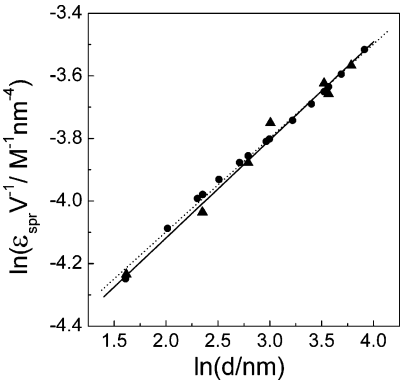

Figure 7. Calculated molar decadic extinction coefficient at the surface plasmon resonance (ϵ_{spr}) per unit volume of gold (V in nm^3) plotted against ln(d) for particle sizes between 5 and 50 nm (circles) and experimental results (triangles). A linear fit to the experimental (theoretical) data is shown as dotted (solid) line.

However, a better agreement between theory and experiment is found if the absorbance ratios are determined in the wavelength region below 600 nm. Figure 6b shows the ratio of the absorbance at the surface plasma resonance peak (A_{spr}) to the absorbance at 450 nm (A_{450}) in dependence of the logarithm of the particle diameter in the size range from 5 to 80 nm. The theoretical data (circles) exhibit an excellent linearity (solid line in Figure 6b; $R^2 > 0.999$), and hence the ratio A_{spr}/A_{450} should be particularly suitable to calculate the particle diameter (in nanometers) from

$$d = \exp\left(B_1 \frac{A_{spr}}{A_{450}} - B_2\right) \qquad (11)$$

Here, B_1 is the inverse of the slope (m) of the linear fit in Figure 6b and $B_2 = B_0/m$ where B_0 is the intercept. Agreement with the experimental data is not perfect, and some spread is observed, resulting in an error of ~18% for the calculation of the particle sizes if the best fit parameters are determined from the *theoretical* data in Figure 6b ($B_1 = 3.55$; $B_2 = 3.11$). If the *experimentally* determined fit parameters are used ($B_1 = 3.00$; $B_2 = 2.20$) the calculation of particle diameters using eq 11 results in an improved average deviation of ~11%. Numerical data of $d(A_{spr}/A_{450})$ which allow the reader to determine the size of GNPs without the need to perform calculations are presented in the Supporting Information.

We found that the particle size can be determined with higher precision if the initial concentration of gold (c_{Au} in mol per liter) used to synthesize the particles is known. In Figure 7, the calculated molar decadic extinction coefficient at the surface plasmon resonance (ϵ_{spr} in M^{-1} nm^{-1}) per unit volume of gold (nm^{-3}) is plotted against ln(d) for particle sizes between 5 and 50 nm. The agreement between theory and experiment is excellent, and the linearity of both experiment ($R^2 = 0.996$) and theory ($R^2 = 0.998$) is striking. The particle diameter (in nanometers) can thus be calculated from c_{Au} (in mol per liter) and the absorbance at the surface plasmon resonance (A_{spr}) according to

(20) Murphy, C. J.; San, T. K.; Gole, A. M.; Orendorff, C. J.; Gao, J. X.; Gou, L.; Hunyadi, S. E.; Li, T. *J. Phys. Chem. B* **2005**, *109*, 13857−13870.
(21) Bogatyrev, V. A.; Dykman, L. A.; Krasnov, Y. M.; Plotnikov, V. K.; Khlebtsov, N. G. *Colloid J.* **2002**, *64*, 671−680.
(22) Rechberger, W.; Hohenau, A.; Leitner, A.; Krenn, J. R.; Lamprecht, B.; Aussenegg, F. R. *Opt. Commun.* **2003**, *220*, 137−141.

$$d = \left(\frac{A_{\mathrm{spr}}(5.89 \times 10^{-6})}{c_{\mathrm{Au}} \exp(C_1)} \right)^{1/C_2} \qquad (12)$$

Here, C_1 and C_2 are parameters calculated from the slope and the intercept in Figure 7 using eq 4, the molar volume (197 cm^3) and the density of gold (19.28 g cm^{-3}). With the use of the theoretical values ($C_1 = -4.70$ and $C_2 = 0.300$) the average error for the calculation of particle sizes according to eq 12 is ~9%. With the use of the experimental values ($C_1 = -4.75$ and $C_2 = 0.314$) this error is reduced to ~6%, and hence eq 12 provides a precise way to calculate the size of particles in the range between 5 and 50 nm.

If the size of the GNPs has been determined by one of the methods described above, then the number density of the particles (N) can be determined from the absorbance of the hydrosol. It was found that the calculated extinction efficiency at 450 nm, can be perfectly fitted with a Gauss function over the whole range of particle sizes ($R^2 = 0.9999$; $\mathrm{CHI}^2 = 10^{-4}$):

$$Q_{\mathrm{ext}} = y_0 + \sqrt{\frac{2}{\pi}} \frac{P}{w} \exp\left[-2\left(\frac{x - x_{\mathrm{c}}}{w} \right)^2 \right] \qquad (13)$$

The fit parameters in eq 13 ($y_0 = -0.866$; $x_{\mathrm{c}} = 96.81$; $w = 110.6$; $P = 553$) can be used to calculate N according to

$$N = \frac{A_{450} \times 10^{14}}{d^2\left[-0.295 + 1.36 \exp\left(-\left(\frac{d - 96.8}{78.2} \right)^2 \right) \right]} \qquad (14)$$

A_{450} is the absorbance at $\lambda = 450$ nm, and d is the particle diameter in nanometer. In Figure 8 the theoretical data of $Q_{\mathrm{ext}}(d)$ are shown as filled circles together with a Gauss fit (solid line) and the experimental data (triangles).

Experimental and theoretical data in Figure 8 are in good agreement, and hence eq 14 affords a rather precise determination of the particle concentration for a known particle diameter, where the average absolute deviation of N determined from eq 14 as compared to the experiment was ~6%. Numerical data of $\epsilon(d)$ at $\lambda = 450$ nm, which allow the reader to determine the concentration of GNPs without the need to perform calculations, are presented in the Supporting Information.

The foregoing results have shown that the GNPs studied experimentally are well described by the theoretical results for uncoated particles. This is understandable, since the GNPs studied here are protected with citrate and/or hydroxylamine. These molecules are small, and it has been shown that citrate adsorbs flat lying on Au(111),[23] which results in a thickness of the protecting layer of merely a few tenths of a nanometer, and hence the GNPs can be described as uncoated in good approximation.

However, it is important to bear in mind that both the surface plasmon resonance maximum (λ_{spr}) and the absorbance ($A(\lambda)$) are dependent on the real refractive index of the surrounding medium (n_{med}) and on the complex refractive index of a coating (n_{coat}), which may be present on the particles' surface. As an example, the influence of n_{med} and n_{coat} on the extinction efficiency at the surface plasmon resonance ($Q_{\mathrm{ext-spr}}$) and on the position of λ_{spr} is shown in Figure 9 for a GNP having a diameter of 20 nm.

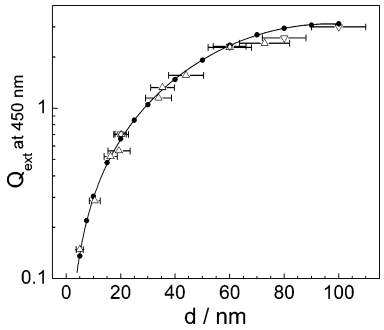

Figure 8. Calculated values of the extinction efficiency of GNPs at a wavelength of 450 nm as a function of the particle diameter (circles). Fit of the theoretical data according to eq 13 (solid line). The experimentally determined data are shown as triangles for comparison.

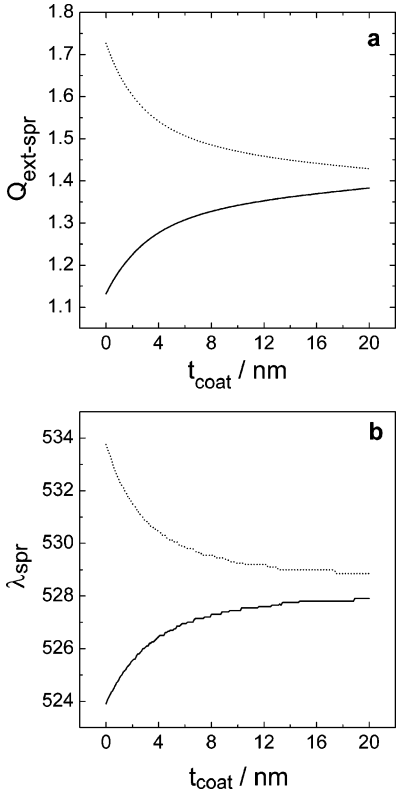

Figure 9. Calculated values of $Q_{\mathrm{ext-spr}}$ (a) and λ_{spr} (b) of a gold nanoparticle (GNP) ($d = 20$ nm), as a function of the thickness (t_{coat}) of the coating layer in water ($n_{\mathrm{med}} = 1.333$, solid lines) and in toluene ($n_{\mathrm{med}} = 1.5$, dotted lines) for a transparent coating ($n_{\mathrm{coat}} = 1.42$; 0).

Figure 9a shows $Q_{\mathrm{ext-spr}}$ as a function of the coating thickness (t_{coat}) in water ($n_{\mathrm{med}} = 1.333$, solid line) and in toluene ($n_{\mathrm{med}} = 1.50$,[24] dotted line) where the n_{coat} value was chosen to be typical for an optically transparent organic compound ($n_{\mathrm{coat}} = 1.42$, 0). In the case of water as the surrounding medium (solid line in Figure 9a) $Q_{\mathrm{ext-spr}}$ increases by ~13% when the coating is 4 nm thick (compared to the uncoated particle). Not surprisingly, $Q_{\mathrm{ext-spr}}$ approaches a value for thicker coatings, which is typical for an uncoated particle in a medium having a real refractive index of

(23) Nichols, R. J.; Burgess, I.; Young, K. L.; Zamlynny, V.; Lipkowski, J. *J. Electroanal. Chem.* **2004**, *563*, 33−39.

(24) Debenham, M.; Dew, G. D. *J. Phys. E: Sci. Instrum.* **1981**, *14*, 544−545.

1.42. In the case of toluene as a surrounding medium $Q_{ext-spr}$ decreases from a relatively large value at $t_{coat} = 0$ by ~11% for a coating thickness of 4 nm and approaches a value of $Q_{ext-spr}$ for thicker coatings which is typical for an uncoated particle in a medium having a real refractive index of 1.42. Similar behavior is observed for λ_{spr}, which increases with increasing t_{coat} when water is the surrounding medium (solid line in Figure 9b) and decreases when toluene is the surrounding medium (dotted line in Figure 9b) to reach the same value for both cases at large coating thickness. This example demonstrates that the influence of a coating and of the surrounding medium on Q_{ext} and hence A cannot be neglected. As a result of that, the equations and/or the fit parameters derived here have to be modified for other dielectric environments.

Another limitation of the methods described here results from the fact that the calculations have been performed for monodisperse and perfectly spherical particles, whereas the experimental data are always collected over a distribution of particle sizes and shapes. As a result of that, the experimentally determined width and position of the surface plasmon resonance may be broadened and/or shifted as compared to the calculations. For example, the position of A_{spr} for oblate particles is shifted to larger wavelength, and hence the corresponding size calculated form eq 10 will be too large, whereas the size calculated from eq 11 will be roughly consistent with the real size. For a broad distribution of particle sizes on the other hand, the size value calculated from eq 10 will be hardly influenced, whereas the size calculated from eq 11 will be too small. These considerations demonstrate that differences between the results of eqs 10 and 11 point to oblate particles and/or to a broad size distribution, whereas consistency of the sizes calculated from eqs 10 and 11 can only be expected for fairly spherical *and* monodisperse particles. However, the particles used here *were* reasonably monodisperse and spherical exhibiting a standard deviation of particle sizes in the range from 10% to 20% of d and an average ratio of the longest to the shortest axis in the range of 1.1 to 1.2. These values are typical for the synthetic procedures described here, and the agreement between experiment and theory was quite good over the whole range of particle diameters (4−100 nm); hence, the particle sizes calculated from eqs 10 and 11 were fairly consistent.

For completeness it should be mentioned that for particle diameters smaller than 10 nm, the calculated absorbance curves did not fit the experiment as well as for larger particles. This may be due to inelastic scattering of conduction electrons at the particle surface and/or to the large fraction of surface atoms. These effects increase with $1/d$, changing the optical functions and the parameters describing the free electron gas. As a result of that inhomogeneous broadening of the surface plasmon resonance and a reduced absorption in the long-wavelength range is observed. Calculations in the size range from 3 to 7 nm should, therefore, be considered as an estimate, and the models presented here should not be applied to particles smaller than 3 nm.

CONCLUSIONS

In summary, it was demonstrated that mean free path corrected Mie theory affords a quantitative description of the absorbance of GNPs in the size range from 5 to 100 nm where a good agreement with the experimental data was found. It was shown that both the size and the concentration of GNPs can be determined directly from UV−vis spectra using eqs 10−13 for the calculation of d and eq 14 for the calculation of N together with the corresponding fit parameters stated in the text. Tabular material presented in the Supporting Information allows the reader to determine size and concentration of GNPs without the need to perform calculations.

ACKNOWLEDGMENT

This work was financially supported by the Biotechnology and Biological Sciences Research Council, the Cancer and Polio Research Fund, the Human Frontiers Science Programme, and the North West Cancer Research Fund. We would like to acknowledge the supply of gold nanoparticles from BBInternational, and we thank A. G. Kanaras, I. E. Sendroju, and S. Romero for the supply of experimental data which helped to confirm the equations presented in this paper.

SUPPORTING INFORMATION AVAILABLE

Additional information as noted in text. This material is available free of charge via the Internet at http://pubs.acs.org.

Received for review February 1, 2007. Accepted March 20, 2007.

AC0702084